Cosmogenic nuclide evidence for enhanced sensitivity of an East Antarctic ice stream to change during the last deglaciation

Duanne A. White, David Fink and Damian B. Gore

This Data Repository contains additional notes on *(1) Methods and procedures* and on *(2) Weathering demarcation and Paleo-ice heights*.

Section (1) covers material relating to sample descriptions (photos in DR figures 1,2 and 3, and tabulated data in DR Table 1), AMS measurements (DR Table 2), cosmogenic exposure age calculations (DR Table 3 and DR Figure 4), and explanatory notes on our field sampling strategy of boulders and bedrock. The second section provides supporting evidence obtained from our two field seasons in the LG-AIS of the 8 weathering demarcation locations from which erratics or cobbles for exposure dating were not available but which are used to reconstruct the paleo-ice sheet profile in conjunction with our exposure age data sets from Ruker, Stinear and Loewe Massifs. DR Figure 5 presents a contour map of modern and calculated paleo-ice thickness contours in the LG-AIS based on various sources. DR Figure 6 shows examples of the weathering demarcation limits at Loewe Massif, Else Platform and Accidental Valley. We provide details of calculations of LG-AIS ice volume reduction since the last deglaciation (~18 ka), and a map of the surficial stratigraphy of Else Platform (DR Figure 7).

(1) Methods and procedures

Thirty transported erratics (either cobbles or large boulders on bedrock, ice-cored moraine or diamict) and four bedrock samples were collected for in-situ cosmogenic exposure dating and processed for ^{10}Be and ^{26}Al from quartz following procedures outlined by Child et al. (2000). Sample locations (maps and photographs) from the Northern Prince Charles Mountains at Loewe Massif (4 erratics), and the Southern Prince Charles Mountains at Mt Stinear/Mt Rymill (15 erratics and 2 bedrock samples) and Mt Ruker (11 erratics and 2 bedrock samples) are presented in DR Figures-1, 2 and 3, respectively. Site description, rock lithology, sample sizes are tabulated in DR Table 1.

Accelerator Mass Spectrometry (AMS) measurements were carried out at the ANTARES AMS Facility at ANSTO, Australia, following methods described by Fink and Smith (2007). Measured ^{10}Be/Be and ^{26}Al/Al ratios (DR Table 2) were corrected by full chemistry procedural blanks, < 10x10^{-15} and < 5x10^{-15}, respectively. Final analytical error in concentrations (atoms/gram quartz) are derived from a quadrature sum of the standard mean error in an AMS ratio, 2% for AMS standard reproducibility, 1% in Be spike assay and 4% error in the ICP-AES Al quartz concentration. Total analytical errors range from 2-5% for ^{10}Be (excluding samples LM-C12a and LM-C14b at 7%) and 4-10% for ^{26}Al atoms/g (excluding 3 samples with errors from 15-20%). The ^{26}Al result for Stin-7a with an error of ~80% resulted from unsatisfactory negative ion-source yield and is considered unreliable.

Standard Reference Material (SRM) for ^{10}Be, NIST-4325, issued by the National Institute of Standards and Technology (NIST, Gaithersburg, Maryland, USA; www.nist.gov) is employed for normalization of all measured ^{10}Be/Be ratios at ANTARES. Recently, Nishiizumi et al., (2007) have revised the nominal ratio of this standard, and inferred a new value for the half-life of ^{10}Be. In this paper, we use the new nominal ^{10}Be/Be ratio for NIST-4325 of 27,900 x 10^{-15}, which is a factor of 1.106 less than the previously accepted value. We also use a ^{10}Be half life of 1.387 ± 0.012 Ma, based on the recent measurements by Korschinek et al. (2010) and Chemleff et al. (2010).

To calculate minimum exposure ages, we employed standard production scaling models for altitude and latitude using algorithms specific for the Antarctic region (Stone, 2000). The use of these new SRM values dictates a further revision of the sea level high latitude (>60° S) production rate for ^{10}Be from 5.10 (which includes a 2.5% production component from muons) to 4.60 ± 0.40 ^{10}Be atoms g^{-1} year^{-1} (see table 6, Balco et al., 2008). For ^{26}Al, we used PRIME Lab ^{26}Al standard Z93-0221 with a nominal ratio value of 16,800x10^{-15} (Fink and Smith, 2007) and convert final ^{26}Al concentrations to exposure age using a ^{26}Al half-life of 0.70 Ma and 30.6 ± 2.7 ^{26}Al atoms g^{-1} year^{-1} (Balco et al., 2008). DR Table-3 presents, scaling factors, site production rates, correction factors and minimum (zero-erosion) exposure ages (columns 8-9) for ^{10}Be and ^{26}Al for each of the three regions sampled. Uncertainties in single-nuclide exposure ages represent propagation of all concentration errors defined above in quadrature with production rate uncertainties of ~9%. Column 10 presents mean boulder age (and standard mean error) derived from a weighted mean of the two single-nuclide isotope ages. We refrain from re-calculating our exposure ages using the 11-15% lower ^{10}Be SLHL production rate proposed by Putnam et al. 2010 derived from a glacial site in the south island of New Zealand. Although our LG-AIS exposure ages would simply scale upwards if applied, to date all similar Antarctic exposure age studies are calibrated against the global SLHL rate used in the paper (i.e. that 4.60 ± 0.40 ^{10}Be atoms g^{-1} year^{-1}). We feel further verification is required in order to accept the Putnam et al. production rate to be representative of the Southern Hemisphere. Importantly, our conclusion regarding deglaciation timing differences between coastal and inland sectors of the LG-AIS is not altered if we apply Putnam's production rate. Similarly, our conclusion that deglaciation in the LG-AIS preceded other areas characterised by slow ice-sheet calving at coastal margins (i.e. the Frames Mountains, Mackintosh et al., 2007) is unaltered because the same production rate and scaling factor changes would also apply. However, the disparity in age between these cosmogenic ages and radiocarbon chronologies, such as from the Wilkes and Mac.Roberson Land coast, would increase, further enhancing our major conclusion that the LG-AIS deglaciated earlier than these regions

Altitude scaling according to methods described by Dunai (2000) using the same adiabatic lapse rate and surface temperature, resulted in exposure ages which are typically 2-4% older. Similarly, scaling factors based on methods labelled as Zreda and Lifton (see Balco et al., 2008 and references therein) resulted, in ages 4-7% and 8-11% respectively older than those given in DR Table 3 – the spread being a function of the altitude range of samples (~200 to 1600 m a.s.l.). Effectively, for Antarctic sites, at a given altitude, different scaling methods agree within the typical range of systematic and analytical errors of AMS measurement and uncertainty in respective SLHL production rates (i.e. age spread of ±5% across all scaling models). Hence the conclusions drawn in this work are independent in the choice of production rate scaling.

Sample thickness ranged from 4-5 cm slices and all ages are corrected taking a mean 4.5 cm thickness (4% age increase using a rock density of 2.7 g/cm^3 and a cosmic ray attenuation length of 150 g/cm^2). Horizon shielding corrections were <4% apart from 6 samples LM-C12a, Stin-8a, Stin-8b, Stin-154b, Stin-154a, and Ruk-192A which required corrections of 4-11%. Shielding measurements were taken every 15° of azimuth interval using a clinometer accurate to 0.5^o elevation.

Site-specific correction factors to production rate variations need to be considered when converting minimum model ages to final exposure ages that best represent the age of deglaciation. Surface weathering, exhumation of a boulder from a moraine, post-depositional re-orientation, and inheritance, particularly in regions affected by cold-based ice, are major issues to consider although they are difficult to quantify accurately (Gosse and Philips, 2001).

Our primary target for sampling were sub-rounded cobbles perched on elevated bedrock, tors or near local summits, similar to the rationale of Fabel et al. (1997) and Bentley et al. (2006).

We consider the sub-rounded cobbles are the most likely to produce the most accurate deglaciation ages for two reasons. First, their shape indicates they have been transported sub-glacially for a considerable distance and thus are highly likely to have been sourced from underneath the outlet glaciers, reducing the probability of preservation of cosmogenic inheritance from any previous irradiation. Second, the bedrock surface provides a more stable platform relative to boulders positioned on matrix-supported or ice-cored moraines which tend to re-orient or re-position boulders during moraine stabilization thus altering their exposure history. Moreover, elevated or even slightly sloped bedrock surfaces reduce the likelihood of extended cover by snow and/or glacial till. Thus, we consider that these samples offer a higher probability of representing unmodified glacial debris following deglaciation. Despite such sampling criteria, numerous other Antarctic publications have encountered sub-populations of samples that have been recycled from older glacial deposits and have not been sufficiently reset, or sub-glacially reworked, buried material, (e.g. Stone et al., 2003, Bentley et al., 2006, Mackintosh et al., 2007). In most circumstances this sub-population is characterised by an inheritance signal readily identified via a depressed (or anomalous) $^{26}Al/^{10}Be$ ratio observed in a dual-isotope plot of the $^{26}Al/^{10}Be$ ratio vs. ^{10}Be (normalized to SLHL), as given in DR figure 4. If pre-irradiation and burial are excessive compared to the duration of the most recent exposure period the apparent ^{26}Al age will be discordant and younger compared to the ^{10}Be age (i.e. Stin-148a, Ruk-251). If burial is short (<200 ka) and undetectable, preservation of a previous exposure period is identified by concordant (within errors) paired ^{10}Be and ^{26}Al ages (i.e. Stin-5a, Stin-7a, Stin-164c, Ruk-192A) statistically inconsistent with the mean age of other samples from the same coeval deposit. Where our preferred sample type was not available (such as in regions of extensive till deposits or ground moraine void of bedrock platforms and boulder-supported stable moraines), we targeted cobbles perched on large, flat boulders that stood above the surrounding basal level of the glacial till or debris. If no acceptable sub-rounded cobbles were available, then the surface of these flat boulders was sampled. The boulders were then selected to avoid areas displaying evidence of surface modification such as from active post-depositional reworking by streams, freeze-thaw, or mass movement.

At four selected sites, a bedrock sample was also collected adjacent to these cobbles to determine the effectiveness of glacial erosion. Removal of surface material from the clasts or bedrock samples through weathering or spalling is considered negligible in most cases due to the presence of glacial polish or striae. Where this is absent, the application of a 0.5 mm/ka erosion rate, typical for most Antarctic environments, would result in a negligible age increase for samples <20 ka and about a 5% increase for ages ~100 ka. Thus, we did not correct ages for an assumed or inferred erosion rate. Corrections due to production rate variations as a function of changes in the paleo-geomagnetic dipole intensity are not required for latitudes greater than about >55° S.

In summary, determining the timing of ice retreat in areas where ice has not produced significant erosion (e.g. in cold based terranes, such as upland Antarctica) is difficult. No sampling criteria is perfect, and even with our preferred sample type it is feasible that we will obtain age reversals with altitude. However, our dataset on the whole is robust, particularly at Loewe Massif where the ages are in stratigraphic order and are consistent with the independent deglaciation timing provided by the onset of biological production at Lake Terrasovoje. At the southern sites, our strike rate is favourable when compared to other sites in Antarctica. Where stratigraphic reversals occur with altitude, samples with the shortest period of exposure at a given elevation are considered to provide the best option for timing of last deglaciation (e.g. Stone et al., 2003; Sugden et al., 2005; White, 2007).

(2) Weathering demarcation lines and paleo ice-heights

Most glacially transported boulders with exposure ages of < 20 ka in the Prince Charles Mountains (Table DR-1 and DR-2; Fink et al., 2006), and in other non-coastal Antarctic ice free

areas with continental climates have been relatively unweathered - i.e. have minor iron staining and tafoni less than a few cm deep (e.g. Fabel et al., 1997; Stone et al., 2003; Ackert and Kurz, 2004; Mackintosh et al., 2007). Thus, the maximum altitude of lightly weathered debris in any one elevation transect can provide a local limit on the elevation of glacial deposition since the global LGM. We consider that the weathering demarcation lines observed in the Prince Charles Mountains represent the former ice surface, rather than englacial boundaries. At all modern ice margins, we observed subglacial debris emanating from the ice surface, even in higher altitude regions where melt was limited. Thus, in the Prince Charles Mountains today, there is no evidence for an englacial boundary above which subglacial debris are not deposited. Also, at many of the sites, a portion of the debris at the LGM demarcation line was supraglacial in character i.e. angular, not striated, and containing lithologies consistent with bedrock at each site.

We identified (from field observations and literature accounts) this glacial limit at ten sites along an ice flow-line in the LG-AIS (DR Figure 5).,These ten locations are named, in a direction from south to north (i.e. co-parallel with ice flow direction) as follows: Mt Menzies (M in DR Figure 5) (Derbyshire and Peterson, 1978; Whitehead and McKelvey, 2002); Mt Ruker (R) (Kolobov, 1980; White and Hermichen, 2007); Rimmington Bluff (RB) (White and Hermichen, 2007); Accidental Valley (AV) (White and Hermichen, 2007); Mt Rymill (Ry) & Mt Stinear (S); Rofe Glacier (Rg); Clemence Massif (C); Fisher Massif (F); Mt Lanyon (L) & Mt Meredith (Me) (Mabin, 1992); Amery Oasis (LM, EP).

Four of these sites - Rofe Glacier, Clemence Massif, Mt Lanyon and Else Platform at Amery Oasis - have not been previously described. The Rofe Glacier & Clemence Massif lie on the northern Mawson Escarpment and were visited by a team of geologists during the PCMEGA expedition of 2002/03, who mapped the maximum height of lightly weathered glacier deposits and recovered samples for comparison with those collected at the sites described in this study. At the Rofe Glacier (68° 19.3'E, 72° 54.5' S), outlet glacier deposits with a similar degree of weathering to the lightly weathered deposits at Mt Stinear were present from the modern glacial margin to a distinct 'bathtub' line at 820 m a.s.l. At Clemence Massif (68° 48.0'E, 71° 13.1'S), no lightly weathered outlet glacier deposits were observed, ~100 m above the height of the present day ice surface. The third, Mt Lanyon, was visited by D. White during the austral field season 2003-2004. Here, no lightly weathered outlet glacier debris was observed between the summit and the distinct band of unweathered debris that reaches ~150 m above the present glacier elevation on the southern side of the massif (see Figure 2 in main text). DR Figures 6 a, b and c, present typical examples of the weathering demarcation limit that identifies the extent of the LGM at Loewe Massif, Else Platform and Accidental Valley, respectively.,

Lastly, the weathering limit at Else Platform forms an extension of the local LGM moraine deposited by the Charybdis Glacier at Loewe Massif (see DR Figure 7), and lies ~ 100 m above the present ice surface height.

Using these observational data sets plus published works that have constrained the extent of LG-AIS ice at various locations during the LGM (see reference list in Fig. DR 5 caption) we have compiled a map of the maximum height of the ice sheet and outlet glaciers during and since the LGM in the LG-AIS (Fig. DR-5). The contours were hand drawn, with the aim of reconstructing a surface consistent with that of the present ice sheet surface morphology, but advanced to fit the available measurements. The resulting surface is similar to recent high-spatial resolution numerical models of the LGM ice sheet in this region (Taylor et al., 2004; Wright et al., 2008). From these contour maps, we constructed a GIS (ARC-GIS 8.2) to create two 3D surfaces (paleo and modern ice heights) from a triangular irregular network, and converted these surfaces to a gridded raster Digital Elevation Model. We then subtracted the modern from the reconstructed surface to calculate the difference in ice volume represented by the LGM and modern ice height in the region down-ice

from the LGM 2500 m elevation contour, or the ice divide where the divide itself was lower than 2500m. The 2500 m contour was chosen for two reasons. First, there are no nunataks that may record paleo-ice heights beyond this contour, so no direct evidence is available. Second, the decrease in the maximum ice thickness since the LGM appears to decrease from the modern grounding line toward the ice divides, which suggests that minimal ice thickening occurred during the LGM beyond this contour, in agreement with proxy evidence of minimal LGM thickening or even lowering in ice cores (Martinerie et al., 1994). Lastly, this volume was then converted to a change in sea level assuming a constant area of 360×10^6 km^2 (Lutgens, 1992).

The estimated sea level contribution (SL), based on the 'best fit' map shown in DR Figure 5 is given by the following expression:

$$SL = 1000*(H_{LGM} - H_{PD})*(A_{LG-AIS}/A_{SL}) = 0.37m$$

Where SL is the equivalent sea level rise in meters, H_{LGM} = the average LGM ice surface height within the area of interest = 1.59 km, H_{PD} = the present day ice surface height within the area of interest = 1.34 km, A_{LG-AIS} = the area of interest within the LG-AIS = 530,000 km^2, and A_{SL} = the area of the global ocean = 360×10^6 km^2.

The accuracy of the sea level estimate was calculated by repeating the mapping and calculations for a 'big ice' and 'small ice' scenario. In both cases, the following parts of the 'best fit' scenario were retained, as we consider these features are constrained by the available data: (1) the grounding line position in Prydz Bay, (2) the 1000 m paleo-surface contour east of the Amery Ice Shelf and north of 70°S is fixed at the same location as in Figure DR 5, and (3) the 1000 m and 2000 m paleo-surface contours on the western side of the basin, from the latitude of Loewe Massif, anticlockwise to the longitude of Mt Stinear.

In the big ice scenario, the 1000 m contour was pushed to the modern grounding line or coastline in areas where there is no former ice height data (i.e. the eastern flank of the Amery Ice Shelf between 70 and 72.5°S, and the western flank north of 70 °S. The 2000 m contour was also pushed further down ice by another ~ 50 km. For the small ice scenario, the 2000 m and 1000 m paleo-ice surface contours were left at their modern positions in these regions. This resulted in sea level estimates of 0.15 and 0.72 m for the small ice and big ice scenarios respectively.

References

Ackert, R., Kurz, M., 2004. Age and uplift rates of Sirius Group sediments in the Dominion Range, Antarctica, from surface exposure dating and geomorphology: Global and Planetary Change, v. 42, p. 207-225.

Balco, G., Stone, J.O., Lifton, N.A., Dunai, T.J., 2008. A complete and easily accessible means of calculating surface exposure ages or erosion rates from [10]Be and [26]Al measurements: Quaternary Geochronology, v3, p. 174-195.

Bentley, M.J., Fogwill, C., Kubik, P.W., Sugden, D.E., 2006. Geomorphological evidence and cosmogenic [10]Be/[26]Al exposure ages for the Last Glacial Maximum and deglaciation of the Antarctic Peninsula Ice Sheet. Geological Society of America Bulletin, v.118, p. 1149-1159.

Chemleff, J., von Blackenburg, F., Kossert, K., Jakob, J., 2010, Determination of the [10]Be half-life by multicollector ICP-MS and liquid scintillation counting. Nuclear Instruments and Methods B, v.268, p 192-199, doi:10.1016/j.nimb.2009.09.012.

Child, D., Elliott G., Misfud, C., Smith A.M., Fink, D., 2000, Sample Processing for Earth Science Studies at ANTARES: Nuclear Instruments and Methods B, v17, p. 856-860.

Derbyshire, E. and Peterson, J.A., 1978, A photo-geomorphic map of the Mt. Menzies nunatak, Prince Charles Mountains, Australian Antarctic Territory: Zeitschrift fur Gletscherkunde und Glazialgeologie, v. 14, p. 17-26.

Domack, E., O'Brien, P., Harris, P., Taylor, F., Quilty, P.G., De Santis, L., Raker, B., 1998, Late Quaternary sediment facies in Prydz Bay, East Antarctica and their relationship to glacial advance onto the continental shelf: Antarctic Science, v. 10(3), p. 236-246, doi: 10.1017/S0954102098000339.

Dunai, T.J., 2000, Scaling factors for production rates of in situ produced cosmogenic nuclides: a critical reevaluation: Earth and Planetary Science Letters, v. 176, p. 157-169.

Fabel, D., Stone, J., Fifield, L.K., Cresswell, R.G., 1997, Deglaciation of the Vestfold Hills, East Antarctica; preliminary evidence from exposure dating of three subglacial erratics, *in* C. Ricci, ed, The Antarctic Region: Geological Evolution and Processes (International Symposium on Antarctic Earth Sciences), v. 7, Terra Antarctica Publication, Siena. pp. 829-834.

Fink, D., and Smith, A.M., 2007, An inter-comparison of ^{10}Be and ^{26}Al AMS reference standards and the ^{10}Be half-life: Nuclear Instruments and Methods B, v259 p.600-609.

Fink, D., McKelvey, B., Hambrey, M.J., Fabel, B., Brown, R., 2006. Pleistocene deglaciation chronology of the Radok Lake basin, Amery Oasis, northern Prince Charles Mountains, Antarctica: Earth and Planetary Science Letters, v.243(1-2), p. 229-243, doi:10.1016/j.epsl.2005.12.006.

Gosse, J.C., and Phillips, F.M., 2001, Terrestrial in-situ cosmogenic nuclides: Theory and Application: Quaternary Science Reviews, v. 20, p. 1475-1560.

Harris, P.T. and O'Brien, P.E., 1998, Bottom currents, sedimentation and ice-sheet retreat facies successions on the Mac Robertson Shelf, East Antarctica: Marine Geology, v. 151, p. 47-72.

Hemer, M. and Harris, P., 2003, Sediment core from beneath the Amery Ice Shelf, East Antarctica, suggests mid-Holocene ice-shelf retreat: Geology, v. 31, p, 127-130.

Hodgson, D.A., Noon, P.E., Vyverman, W., Bryant, C.L., Gore, D.B., Appleby, P., Gilmour, M., Verleyen, E., Sabbe, K., Jones, V.J., Ellis-Evans, J.C., Wood, P.B., 2001, Were the Larsemann Hills ice-free through the last glacial maximum? Antarctic Science, v. 13, p. 440-454

Kolobov, D.D., 1980, Rel'yef gory Ruker (yuzhnaya chast' gor Prins-Charl'z, Vostochnaya Antarktida). Relief of Mount Ruker, southern Prince Charles Mountains, East Antarctica: Trudy Sovetskoy Antarkticheskoy Ekspeditsiy, v. 70, p. 66-75.

Korschinek, G., Bergmaier, A., Faestermann, T., Gerstmann, U.C., Knie, K., Rugel, G., Wallner, A., Dillman, I., Dollinger, G., von Gostomski, Lierse Ch., Kossert, K., Maitia, M., Poutivtsev, M., Remmert, A., 2010, A new value for the half-life of ^{10}Be by heavy ion elastic recoil detection and liquid scintillation counting. Nuclear Instruments and Methods, v.268, p.187–191, doi:10.1016/j.nimb.2009.09.020.

Leventer, A., Domack, E., Dunbar, R., Pike, J., Stickley, C., Maddison, E., Brachfeld, S., Manley, P., McClennen, C. 2006, Marine sediment record from the East Antarctic margin reveals dynamics of ice sheet recession: GSA Today v. 16(12), p. 4-10, doi: 10.1130/GSAT01612A.1.

Lilly, K, Fink, D., Fabel, D., Lambeck, K. ,2010. Pleistocene dynamics of the interior East Antarctic ice sheet, Geology, v. 38, p. 703-706.

Lutgens, F.K., 1992. Essentials of Geology. MacMillan, New York,: 269 pp.

Martinerie, P., Lipenkov, V.Y., Raynaud, D., Chappellaz, J., Barkov, N.I. and Lorius, C., 1994. Air Content Paleo Record in the Vostok Ice Core (Antarctica) - a Mixed Record of Climatic and Glaciological Parameters: Journal of Geophysical Research-Atmospheres, v. 99, p. 10565-10576.

Masarik, J., and Weiler, R., 2003, Production rates of cosmogenic nuclides in boulders: Earth and Planetary Science Letters, v. 216, p. 201–208.

Mabin, M.C.G., 1992. Late Quaternary ice-surface fluctuations of the lower Lambert Glacier, northern Prince Charles Mountains. In: Y. Yoshida (Editor), Recent Progress in Antarctic Earth Science. Terra Scientific Publishing Company, Tokyo, pp. 683-687.

Mackintosh, A., White, D., Fink, D., Gore, D., 2007. Exposure ages from mountain dipsticks in Mac.Robertson Land, East Antarctica, indicate little change in ice sheet thickness since the Last Glacial Maximum: Geology, v.35, p. 551–554; doi: 10.1130/G23503A.1.

Nishiizumi, K, Mineo, I., Caffee, M., Southon, J., Finkel, R.,and McAninch, J., 2007, Absolute Calibration of [10]Be Standards: Nuclear Instruments and Methods, B, v. 258, p. 403-413.

Powers, M.C., 1953. A new roundness scale for sedimentary particles. Journal of Sedimentary Petrology, 23: 117-119.

Putnam, A.E., Schaefer, J.M., Vandergoes, M., Barrell, D.J.A., Denton, G.H., Kaplan, M.R., Schwartz, R., Finkel, R.C., Goehring, B.M., and Kelley, S.E., 2010.,In situ cosmogenic [10]Be production rate from the Southern Alps, New Zealand. Quaternary Geochronology, doi:10.1016/j.quageo.2009.12.001.

Stone, J.O., 2000, Air pressure and cosmogenic isotope production: Journal of Geophysical Research, 105(B10), p. 23,753-23,759, doi: 10.1029/2000JB900181.

Stone, J.O., Balco, G.A., Sugden, D.E., Caffee, M.W., Sass, L.C., Cowdery, S.G., and Siddoway, C., 2003, Holocene Deglaciation of Marie Byrd Land, West Antarctica: Science, v. 299, p. 99-102.

Sugden, D.E., Balco, G., Cowdery, S.G., Stone, J., Sass, L.C., 2005, Selective glacial erosion and weathering zones in the coastal mountains of Marie Byrd Land, Antarctica: Geomorphology, v. 67(3-4), p. 317-334, doi: 10.1016/j.geomorph.2004.10.007.

Taylor, F. and McMinn, A., 2002, Late Quaternary diatom assemblages from Prydz Bay, Eastern Antarctica: Quaternary Research, v. 57, p. 151-161

Taylor, J., Siegert, M.J., Payne, A.J., Hambrey, M.J., O'Brien, P.E., Cooper, A.K. and Leitchenkov, G., 2004. Topographic controls on post-Oligocene changes in ice sheet dynamics, Prydz Bay region, East Antarctica: Geology, v. 32, p. 197-200.

White, D., 2007, Cenozoic Glacial History and Landscape Evolution of Mac.Robertson Land and the Lambert Glacier-Amery Ice Shelf System, East Antarctica, Ph.D., Thesis, Dept of Physical Geography, Macquarie University (unpublished).

White, D.A. and Hermichen, W-D, 2007, Glacial and Periglacial History of the Southern Prince Charles Mountains, East Antarctica. Terra Antarctica, 14(1), 5-12.

Whitehead, J.M., McKelvey, B.C., 2002. Cenozoic glacigene sedimentation and erosion at the Menzies Range, southern Prince Charles Mountains, Antarctica: Journal of Glaciology, v. 48(161), p. 226-236.

Wright A.P., White, D.A., Gore, D.B. and Siegert, M.J. 2008. Antarctica at the Last Glacial Maximum, Deglaciation and the Holocene. *In* F. Florindo and M. Siegert, ed., Antarctic Climate Evolution, Elsevier. pp. 531-570.

Zwartz, D., Bird, M.I., Stone, J. and Lambeck, K., 1998, Holocene sea-level change and ice-sheet history in the Vestfold Hills, East Antarctica: Earth and Planetary Science Letters, v. 155, p. 131-145.

Data Repository: Table DR1

Site location and sample description from Northern (N) and Southern (S) Prince Charles Mountains (PCM), East Antarctica. Samples are listed in decreasing order of sample elevation referenced to the nearest outlet glacier ice margin (*see DR Table 3 for details). Mt Ruker samples in italics are above the weathering demarcation altitude. R and S refer to the roundess (Powers, 1953) and presence (None, Some, Few) of striae on the sample.

sample name	lat. long. ºS ºE		m above outlet glacier*	alt (m)	sample size (cm) A	B	C	bedrock sample lithology	lithology	R	S	position	weathering
Loewe Massif (NPCM)													
LM-C12a	-70.5356	67.8000	229	329	200	150	100	charnockite	charnockite	A	N	boulder on moraine	moderate
LM-C8b	-70.5464	67.9614	162	242	20	10	10	charnockite	psammite	SR	N	cobble on moraine	little to none
LM-C3	-70.5166	68.0044	116	156	30	20	20	charnockite	psammite	SR	S	cobble on large boulder on diamict	minor staining
LM-C14b	-70.526	67.8676	66	211	30	20	10	charnockite	psammite	A	N	cobble on bedrock	minor staining
Mt Stinear (SPCM)													
Rym-173	-73.015	65.9051	393	993	200	150	100	granite	fels. gneiss	A	N	boulder on diamict	minor staining
Stin-164a	-73.0154	66.5117	392	592	10	10	10	granite	fels. gneiss	SR	N	cobble on bedrock	minor staining
Stin-164b	-73.0154	66.5117	392	592	10	10	10	granite	quartzite	SR	N	cobble on bedrock	minor staining
Stin-164c	-73.0154	66.5117	392	592	N/A	N/A	N/A	granite	quartz vein	N/A	N	bedrock	minor staining
Stin-117	-73.0464	66.4811	361	521	600	400	200	fels. gneiss	pelite	A	N	boulder on ice cored diamict	minor staining
Stin-154a	-73.0597	66.3251	145	705	20	10	10	fels. gneiss	quartzite	SR	N	cobble on bedrock	minor staining
Stin-154b	-73.0593	66.3255	140	700	15	15	10	fels. gneiss	quartzite	SR	N	cobble on bedrock	minor staining
Stin-147b	-73.002	66.535	120	320	10	10	10	granite	quartzite	SR	N	cobble on bedrock	minor staining
Stin-147c	-73.002	66.535	120	320	30	20	20	granite	quartzite	SR	N	cobble on thin diamict	minor staining
Stin-140	-73.075	66.4645	110	310	200	100	100	fels. gneiss	quartzite	SA	N	boulder on ice cored diamict	minor staining
Stin-6a	-73.0061	66.4899	95	535	30	20	10	granite	quartzite	SR	N	cobble on bedrock	minor staining
Stin-8a	-73.0749	66.2883	85	670	15	10	10	fels. gneiss	quartzite	SR	N	cobble on bedrock	minor staining

Sample	Long	Lat						Lithology	Lithology			Setting	Weathering
Stin-8b	-73.0749	66.2883	85	670	N/A	N/A	N/A	fels. gneiss	fels. gneiss	N/A	F	polished bedrock	minor staining
Stin-5a	-73.0088	66.4491	81	561	5	5	5	granite	quartzite	SA	N	cobble on bedrock	mod. staining
Stin-7a	-73.0749	66.2845	71	551	30	30	20	granite	quartzite	SR	F	cobble on bedrock	minor staining
Stin-139	-73.0702	66.4805	70	260	300	200	100	fels. gneiss	quartzite	SA	N	boulder on ice cored diamict	minor staining
Stin-148a	-72.9994	66.5463	40	240	10	10	5	granite	quartzite	SA	F	cobble on bedrock	very little
Mt Ruker (SPCM)													
Ruk-249	*-73.6398*	*64.3054*	*425*	*1655*	*25*	*25*	*15*	*metabasalt*	*quartzite*	*A*	*N*	*cobble on ice cored diamict*	*minor staining*
Ruk-251	*-73.6287*	*64.2957*	*395*	*1525*	*80*	*60*	*60*	*metabasalt*	*quartzite*	*A*	*N*	*boulder on ice cored diamict*	*minor staining*
Ruk-244	*-73.5979*	*64.36*	*272*	*1502*	*100*	*100*	*60*	*metabasalt*	*fels. gneiss*	*A*	*N*	*boulder on ice cored diamict*	*minor staining*
Ruk-227	*-73.5817*	*64.4802*	*200*	*1280*	*300*	*200*	*200*	*metabasalt*	*fels. gneiss*	*A*	*N*	*boulder on ice cored diamict*	*minor staining*
Ruk-258A	*-73.6244*	*64.2028*	*180*	*1410*	*25*	*25*	*20*	*metabasalt*	*fels. gneiss*	*SR*	*N*	*cobble on bedrock*	*minor staining*
Ruk-199A	-73.6137	64.2758	150	1340	30	20	10	metabasalt	fels. gneiss	R	S	cobble on bedrock	none
Ruk-199C	-73.6137	64.2758	150	1340	N/A	N/A	N/A	metabasalt	quartz vein	N/A	N	bedrock spur	very crumbled
Ruk-192A	-73.5802	64.5248	145	1195	25	20	20	metabasalt	fels. gneiss	R	N	cobble on bedrock	minor staining
Ruk-235A	-73.6244	64.1901	140	1370	15	15	10	metabasalt	fels. gneiss	R	S	cobble on bedrock	none
Ruk-235B	-73.6244	64.1901	140	1370	20	15	10	metabasalt	fels. gneiss	R	N	cobble on bedrock	minor staining
Ruk-235C	-73.6244	64.1901	140	1370	N/A	N/A	N/A	metabasalt	quartz vein	N/A	N	bedrock spur	very crumbled
Ruk-261b	-73.5463	64.6134	129	1239	30	30	20	granite	fels. gneiss	R	S	cobble on large boulder on felsemeer	none
Ruk-201	-73.6119	64.2755	101	1291	20	20	15	metabasalt	fels. gneiss	R	S	cobble on bedrock	none

Data Repository: Table DR2

AMS measurement results for $^{10}Be/Be$ and $^{26}Al/Al$ ratios and other relevant data. Mt Ruker samples in italics are above the weathering demarcation altitude.

Sample name	Sample quartz mass (g)	Be carrier mass (mg) (1)	Al conc (ppm) (2)	$^{10}Be/Be$ (x 10^{-15}) (3)	Analytical error (%) (4)	^{10}Be conc (atoms/g-Q) (x10^3) (5)	$^{26}Al/Al$ (x 10^{-15}) (3)	Analytical error (%) (4)	^{26}Al conc (atoms/g-Q) (x10^3) (5)	$^{26}Al/^{10}Be$ conc. ratio (6)
Loewe Massif (NPCM)										
LM-C12a	33.6	0.424	88.8	153.9	7.1	129.8 ± 9.6	528.4	7.4	1047 ± 92	8.1 ± 0.9
LM-C8b	28.1	0.388	177.0	119.6	4.7	110.4 ± 5.7	181.7	14.6	717 ± 110	6.5 ± 1.1
LM-C3	54.9	0.419	199.3	184.8	5.2	94.2 ± 5.4	139.0	10.9	618 ± 73	6.6 ± 0.9
LM-C14b	22.2	0.369	91.7	73.5	7.3	81.7 ± 6.3	275.4	11.1	564 ± 68	6.9 ± 1.0
Mt Stinear (SPCM)										
Rym-173	80.3	0.405	110.6	885.8	1.6	298.6 ± 8.2	824.8	8.8	2036 ± 202	6.9 ± 0.7
Stin-164a	61.8	0.405	140.1	228.4	3.9	100.0 ± 4.5	187.1	31	585 ± 183	5.9 ± 1.9
Stin-164b	66.5	0.335	17.7	307.9	2.9	103.7 ± 3.8	1980	6.3	782 ± 61	7.6 ± 0.7
Stin-164c	80.0	0.404	65.7	8733	3.4	2948 ± 119	10800	4.3	15840 ± 1000	5.4 ± 0.4
Stin-117	80.7	0.410	66.9	515.0	2.6	174.9 ± 6.0	758.2	7.5	1132 ± 100	6.5 ± 0.6
Stin-154a	81.9	0.407	308.7	339.6	3.5	112.8 ± 4.7	147.3	35	1015 ± 362	9.0 ± 3.2
Stin-154b	83.4	0.402	172.8	361.2	5.5	116.4 ± 6.9	224.1	9.9	864 ± 94	7.4 ± 0.9
Stin-147b	81.2	0.409	60.9	230.3	6.0	77.5 ± 4.9	418.3	11	569 ± 70	7.3 ± 1.0
Stin-147c	79.8	0.409	557.6	229.1	5.6	78.5 ± 4.7	23	64	289 ± 187	3.7 ± 2.4
Stin-140	52.0	0.402	52.5	135.9	5.4	70.2 ± 4.1	472.9	10	554 ± 62	7.9 ± 1.0
Stin-6a	80.2	0.395	151.1	259.2	3.7	85.3 ± 3.7	172.7	15	582 ± 93	6.8 ± 1.2
Stin-8a	73.0	0.402	298	264.3	3.3	97.3 ± 3.9	72	32	480 ± 155	4.9 ± 1.6
Stin-8b	20.4	0.403	1013	70.3	7.3	92.8 ± 7.1	<13	-	< 300	-
Stin-5a	80.0	0.416	48.5	1193.6	1.6	415 ± 11.4	2574	10	2787 ± 316	6.7 ± 0.8
Stin-7a	41.2	0.599	1167	865.8	3.8	841.3 ± 37.3	50	82	1300 ± 1070	(1.6 ± 1.3)
Stin-139	25.9	0.405	148.8	83.8	6.2	87.5 ± 5.7	133.3	20	443 ± 89	5.1 ± 1.1
Stin-148a	49.8	0.400	207.9	284.9	3.2	152.9 ± 6.0	144.4	20	670 ± 138	4.4 ± 0.9
Mt Ruker (SPCM)										
Ruk-249	*83.7*	*0.393*	*180.6*	*10737*	*0.6*	*3370 ± 78*	*5007*	*4.9*	*20190 ± 1360*	*6.0 ± 0.4*

Ruk-251	79.8	0.408	79.1	4697	1.2	1605 ± 41	3771	4.3	6659 ± 421	4.1 ± 0.3
Ruk-244	31.9	0.332	26.5	2736	1.1	1903 ± 48	18320	4.3	10840 ± 680	5.7 ± 0.4
Ruk-227	31.7	0.380	51.8	3540	1.2	2836 ± 71	13930	3.3	16100 ± 910	5.7 ± 0.4
Ruk-258A	81.5	0.402	18.3	1464.3	1.5	482.7 ± 13.0	8320	4.5	3399 ± 219	7.0 ± 0.5
Ruk-199A	63.2	0.403	17.8	610.5	2.1	260.2 ± 8.0	4512	4.9	1793 ± 120	6.9 ± 0.5
Ruk-199C	55.1	0.409	25.9	1218.6	1.5	604.5 ± 16.3	6268	2.9	3624 ± 196	6.0 ± 0.4
Ruk-192A	81.2	0.405	21.7	1411.9	1.4	470.7 ± 12.4	6237	5.6	3021 ± 218	6.4 ± 0.5
Ruk-235A	81.6	0.409	75.8	520.7	2.5	174.4 ± 5.8	676.8	5.9	1145 ± 86	6.6 ± 0.5
Ruk-235B	57.4	0.404	15.0	1098.2	4.5	516.6 ± 25.8	10970	2.8	3674 ± 198	7.1 ± 0.5
Ruk-235C	62.8	0.405	18.5	761.0	2.5	328.0 ± 11.1	5200	5.2	2147 ± 149	6.6 ± 0.5
Ruk-261b	62.9	0.373	16.9	446.6	3.0	177.0 ± 6.7	3211	5.5	1211 ± 87	6.7 ± 0.6
Ruk-201	60.1	0.405	20.3	348.3	3.2	156.9 ± 6.2	2564	5.8	1162 ± 86	7.4 ± 0.6

Footnotes: DR Table 2

1. Be carrier determined by mass from an ICP (MERCK) calibration solution at 1000 ± 3 ppm (mg/L)
2. Al concentration measured by ICP-AES. A representative error of ± 4% is assigned to all ICP results and added in quadrature with other analytical errors for final error in [26]Al concentrations.
3. Weighted mean isotopic ratio of repeat AMS measurements (via counting statistics and normalisation errors) determined after chemistry blank subtraction and normalization to AMS standards in use at the ANTARES AMS facility (PRIME-Z93-0221 for [26]Al/Al, nominal value = 16,800 x 10^{-15} ; NIST-4325 for [10]Be/Be, nominal value = 27,900 x 10^{-15}).
   Chemistry procedural blanks prepared from commercially purchased 1000 ppm Be and Al calibration solutions resulting in [10]Be/Be ~ (5-15) x 10^{-15} and [26]Al/Al ~ (<10) x 10^{-15}.
4. Error in mean AMS ratio determined as the larger of the mean standard deviation or weighted mean error.
5. Cosmogenic radioisotope concentration at site location. Uncertainty represents quadrature addition of 1σ errors in final AMS ratio, quartz mass, Al assay and a 2% systematic variability in repeat measurement of AMS standards (see Fink and Smith, 2007).
6. Isotope concentration ratio. Error based on quadrature addition of only individual analytical isotope errors. Value for Stin-7a in parenthesis due to doubtful reliability of [26]Al result which performed poorly during AMS measurement.

Data Repository: Table DR3

Exposure age results for Loewe Massif, Mt Stinear and Mt Ruker. Note that samples are listed in decreasing height above current height of outlet glacier. Mt Ruker samples in italics are above the weathering demarcation altitude.

Sample name	Alt (m)	Ice edge altitude (m)	Height above outlet glacier (m) (1)	Scaling factor (2)	Horizon shielding (3)	^{10}Be prod. rate (at/g/yr) (4)	^{26}Al prod. rate (at/g/yr) (4)	^{10}Be min exposure age (ka) (5)	^{26}Al min exposure age (ka) (5)	Mean exposure age (ka) (6)
Loewe Massif,(NPCM)										
LM C12a	329	100	229	1.742	0.960	7.39	49.92	17.7 ± 1.6	21.2 ± 2.1	18.9 ± 1.7
LM C8b	242	80	162	1.597	1.000	7.05	47.68	15.7 ± 1.2	15.2 ± 2.4	15.6 ± 1.1
LM C3	156	40	116	1.463	1.000	6.46	43.67	14.6 ± 1.2	14.3 ± 1.8	14.5 ± 1.0
LM C14b	211	145	66	1.548	1.000	6.84	46.22	12.0 ± 1.1	12.3 ± 1.6	12.1 ± 0.9
Mt Stinear (SPCM)										
Rym-173	993	600	393	3.207	0.989	14.01	94.70	21.4 ± 1.4	21.7 ± 2.4	21.5 ± 1.2
Stin-164a	592	200	392	2.240	0.999	9.88	66.81	10.1 ± 0.7	8.8 ± 2.7	10.1 ± 0.7
Stin-164b	592	200	392	2.240	0.999	9.88	66.81	10.5 ± 0.7	11.8 ± 1.1	10.9 ± 0.6
Stin-164c	592	200	392	2.240	0.999	9.88	66.81	323 ± 24	270 ± 26	298 ± 26, *
Stin-117	521	160	361	2.096	0.975	9.02	61.01	19.5 ± 1.3	18.7 ± 1.9	19.2 ± 1.1
Stin-154a	705	560	145	2.474	0.890	9.72	66.03	11.6 ± 0.7	15.5 ± 4.8	11.7 ± 0.7
Stin-154b	700	560	140	2.485	0.900	9.88	66.47	11.8 ± 0.9	13.1 ± 1.4	12.2 ± 0.7
Stin-147b	320	200	120	1.727	0.999	7.62	51.50	10.2 ± 0.9	11.1 ± 1.5	10.4 ± 0.7
Stin-147c	320	200	120	1.727	0.999	7.62	51.50	10.3 ± 0.8	(5.6 ± 3.5)	10.3 ± 0.8, &
Stin-140	310	200	110	1.710	0.967	7.30	49.36	9.6 ± 0.8	11.3 ± 1.3	10.0 ± 0.7
Stin-6a	535	440	95	2.124	0.997	9.35	63.22	9.1 ± 0.7	9.3 ± 1.5	9.2 ± 0.6
Stin-8a	670	585	85	2.407	0.891	9.47	64.03	10.3 ± 0.6	7.5 ± 2.1	10.1 ± 0.8
Stin-8b	670	585	85	2.407	0.891	9.47	64.03	9.8 ± 0.8	(<, 5)	9.8 ± 0.8, &*
Stin-5a	561	480	81	2.176	0.999	9.60	64.91	43.7 ± 2.8	43.9 ± 5.5	43.7 ± 2.5
Stin-7a	551	480	71	2.156	0.999	9.51	64.30	90.5 ± 6.7	(21 ± 16)	90.5 ± 6.7 &
Stin-139	260	190	70	1.627	0.972	6.98	94.70	12.6 ± 1.1	9.4 ± 1.9	11.8 ± 1.4
Stin-148a	240	200	40	1.594	0.997	7.02	47.45	21.9 ± 1.5	14.2 ± 2.9	Complex ^

Mt Ruker (SPCM)

Sample										
Ruk-249	*1655*	*1230*	*425*	*5.497*	*0.995*	*24.15*	*163.3*	*145 ± 9*	*132 ± 12*	*140 ± 7*
Ruk-251	*1525*	*1230*	*395*	*4.970*	*0.998*	*21.90*	*148.1*	*74.6 ± 4.8*	*46.0 ± 3.9*	*Complex ^*
Ruk-244	*1502*	*1230*	*272*	*4.881*	*1.000*	*21.55*	*145.7*	*90.3 ± 5.8*	*77.3 ± 6.7*	*84.7 ± 6.5*
Ruk-227	*1280*	*1080*	*200*	*4.083*	*0.998*	*18.00*	*121.7*	*164 ± 11*	*142 ± 12*	*154 ± 11*
Ruk-258A	*1410*	*1230*	*180*	*4.537*	*0.989*	*19.82*	*134.0*	*24.5 ± 1.6*	*25.7 ± 2.0*	*24.9 ± 1.3*
Ruk-199A	1340	1190	150	4.288	0.970	18.37	124.2	14.2 ± 0.9	14.5 ± 1.2	14.3 ± 0.7
Ruk-199C	1340	1190	150	4.288	0.970	18.37	124.2	33.2 ± 2.1	29.6 ± 2.3	31.6 ± 1.8 *
Ruk-192A	1195	1050	145	3.806	0.955	16.05	108.5	29.5 ± 1.8	28.2 ± 2.5	29.1 ± 1.5
Ruk-235A	1370	1230	140	4.394	0.995	19.30	130.5	9.1 ± 0.6	8.8 ± 0.8	9.0 ± 0.5
Ruk-235B	1370	1230	140	4.394	0.995	19.30	130.5	26.9 ± 2.0	28.5 ± 2.2	27.7 ± 1.5
Ruk-235C	1370	1230	140	4.394	0.995	19.30	130.5	17.1 ± 1.1	16.6 ± 1.5	16.9 ± 0.9,*
Ruk-261b	1239	1100	129	3.948	0.999	17.42	117.8	10.2 ± 0.7	10.3 ± 0.9	10.2 ± 0.6
Ruk-201	1291	1190	101	4.120	0.989	18.00	121.7	8.7 ± 0.6	9.6 ± 0.9	9.0 ± 0.5

Footnotes: DR Table 3

1. Height of sample above present day surface of outlet glaciers deduced from difference in sample altitude above sea level and modern altitude of proximal glacier surface
2. Altitude and latitude scaling factors, including modifications for Antarctic pressure-altitude relationship, from Stone (2000)
3. Corrections for horizon shielding following methods of Masarik and Weiler (2003) using m = 2.65. Corrections for paleo-geomagnetic field variations at 73° S are not applicable. Corrections for seasonal snow cover not included.
4. Site production rate based on sea-level, high latitude spallogenic plus muon (2.5%) production rates of ^{10}Be = 4.60 ± 0.40 atoms/g.y and ^{26}Al = 30.6 ± 2.7 atoms/g.y (Balco et al., 2008). Production corrections for sample thickness assume all samples were 4-5 cm thick using a density ρ = 2.7 g/cm^3 and a cosmic ray mean attenuation path length Λ = 150 g/cm^2.
5. Minimum exposure ages based on ^{10}Be half-life = 1.387 Ma and ^{26}Al half-life = 0.72 Ma. Correction for rock surface erosion rate not included. Single isotope age errors propagated from concentration error with additional error of 9% in production rate.
6. Boulder age taken as the weighted mean age of individual isotope ^{10}Be and ^{26}Al ages. Final age error per boulder taken as the standard error in the mean. 'Complex' denotes a sample whose paired isotope ages are considered to be inconsistent with continuous, simple exposure having discordant ages as a result of long term burial prior to last exposure.
   * Bedrock samples Stin-164c, Stin-8b, Ruk-199C, Ruk-235C
   & Boulder age for Stin-7a, -8b and -147c given by ^{10}Be age only due to unacceptable errors (and ages) in ^{26}Al age;
   ^ Stin-148a and Ruk-251 designated as 'complex' as the paired ^{10}Be-^{26}Al age difference is outside a 2σ overlap.

Data Repository Figure DR1 : Sample sites for exposure dating from Loewe Massif, Northern Prince Charles Mountains
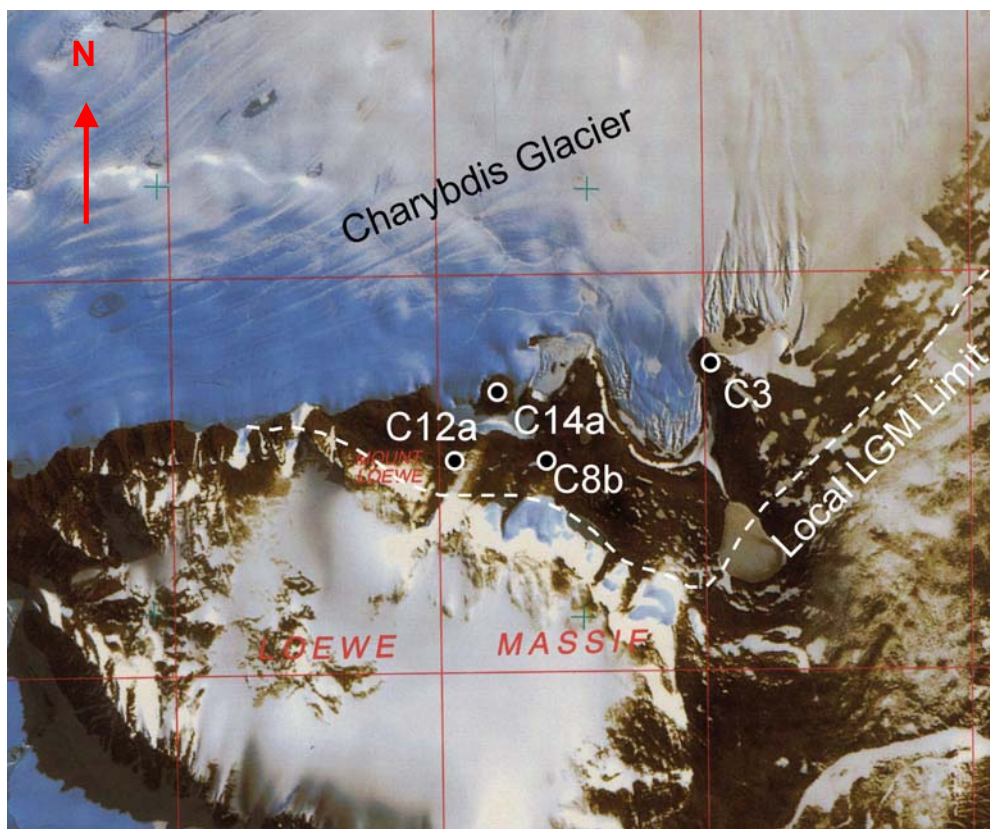

Fig DR1a: Aerial view of location of the 4 post-LGM samples from Loewe Massif. Lake Terrasovoja is the large pear shaped lake to the right of centre of photo. The white dashed line identifies the LGM limits determined from field mapping. The red vertical lines are approximately 5 km apart.
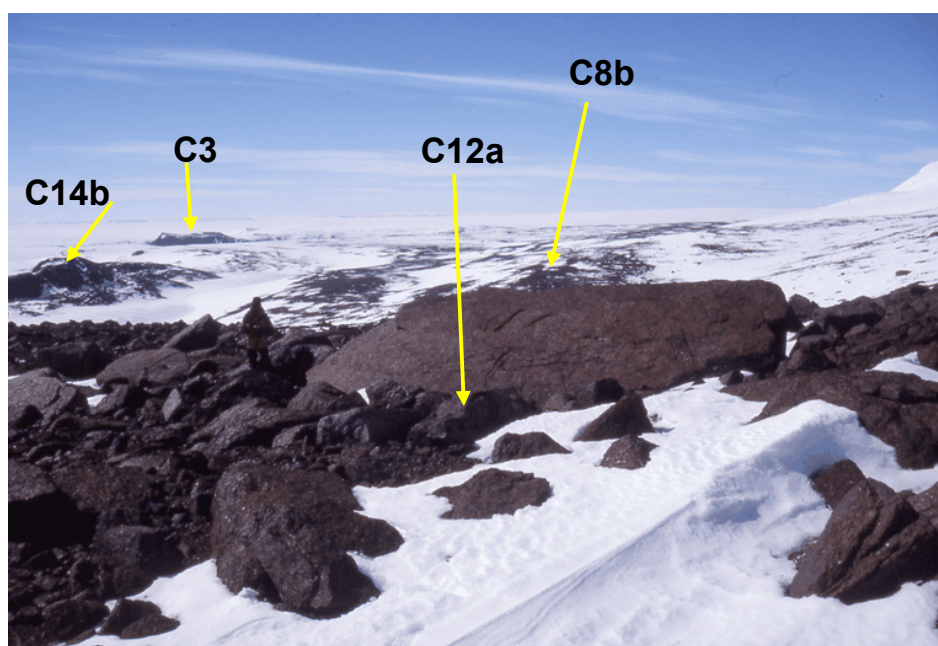
Fig DR1b: Overview of relative positions of sample sites with NPCM-LM-C12a in the foreground. Looking due east
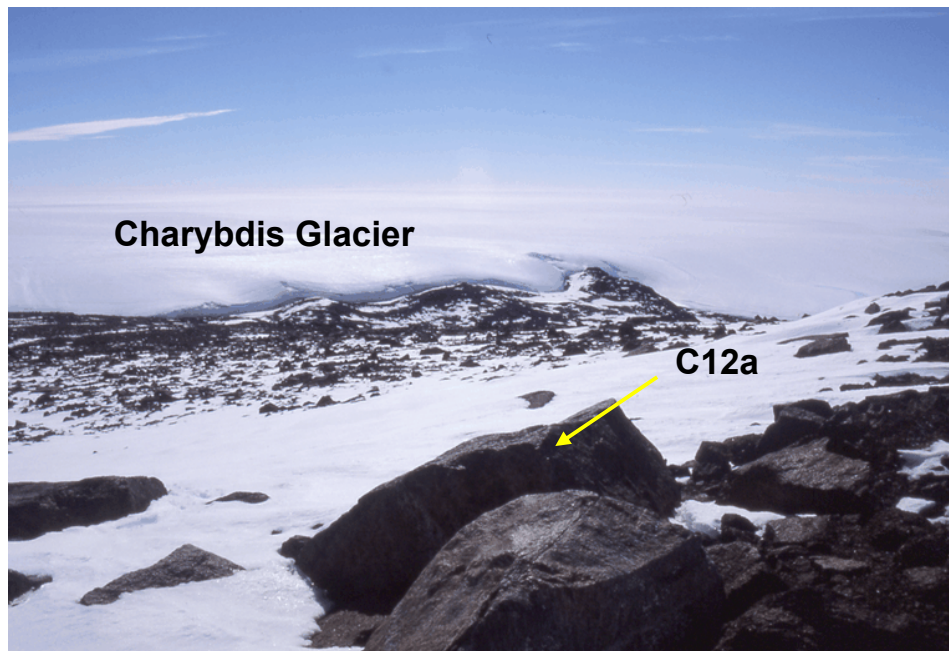
Fig DR1c: View of sample NPCM-LM-C12a (altitude 329 m) looking towards   Charybdis Glacier

Fig DR1d: Location and close-up for sample NPCM-LM-C3 (156 m)

Fig DR1e: Site location for NPCM-LM-C8b (242 m)

Supplementary Figure DR2: Sample sites for exposure dating from Mt Stinear, Southern Prince Charles Mountains.

Site locations are given whole numbers (e.g. 154). At sites where multiple samples were collected, each sample is labelled with a lowercase letter suffix – e.g. 154a, 154b etc. Where only one sample was collected at each site, it is labelled with the site number only.
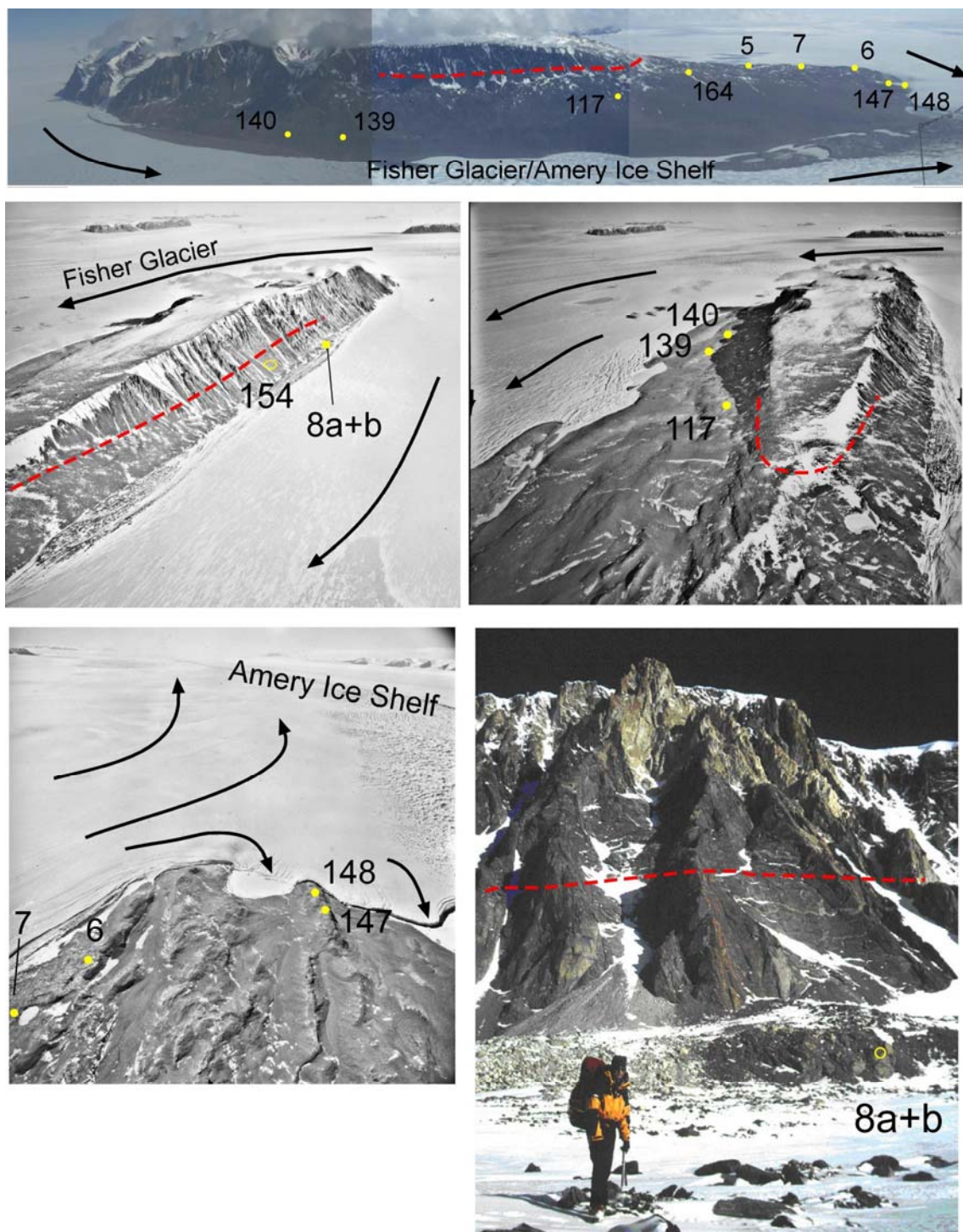
Fig DR2a: Aerial views of location of sample sites from Mt Stinear taken from above the Amery Ice Shelf. The length of the massif is ~20 km and the height of the outlet glaciers during their last advance is marked by the dashed red line. Clockwise from top: from NW, 20/1/03; oblique from N, March 1959, ANT71 9120R; from W towards Edwards Pillar, 12/12/02; northern tip of massif, looking N, January 1959, ANT63 7222L; western flank, looking SE, March 1959, ANT71 9125R.
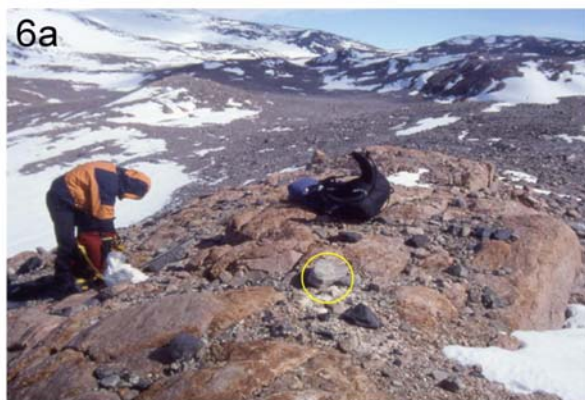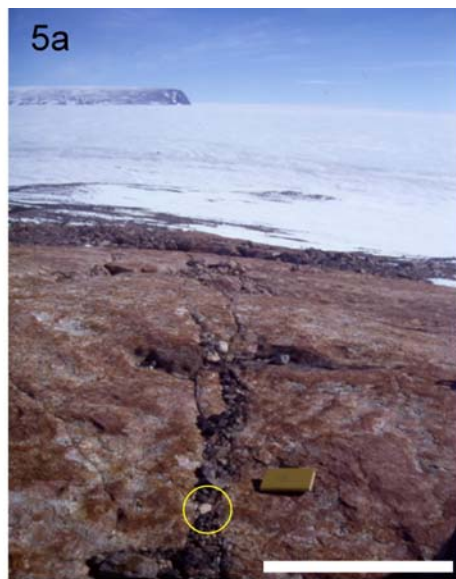
Fig DR2b. Selected sample site photos. Circles indicate sampled cobbles, arrows show position of sampled boulder surface. Scale bars are 1 m long.
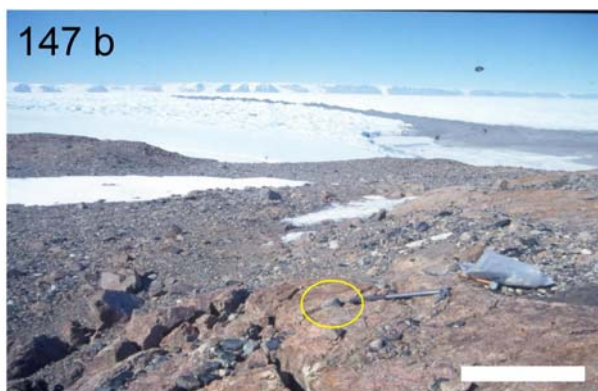
Fig DR2c: Selected sample site photos. Circles indicate sampled cobbles. Scale bars are 1 m long.

Supplementary Figure DR3: Sample sites for exposure dating from Mt Ruker, Southern Prince Charles Mountains
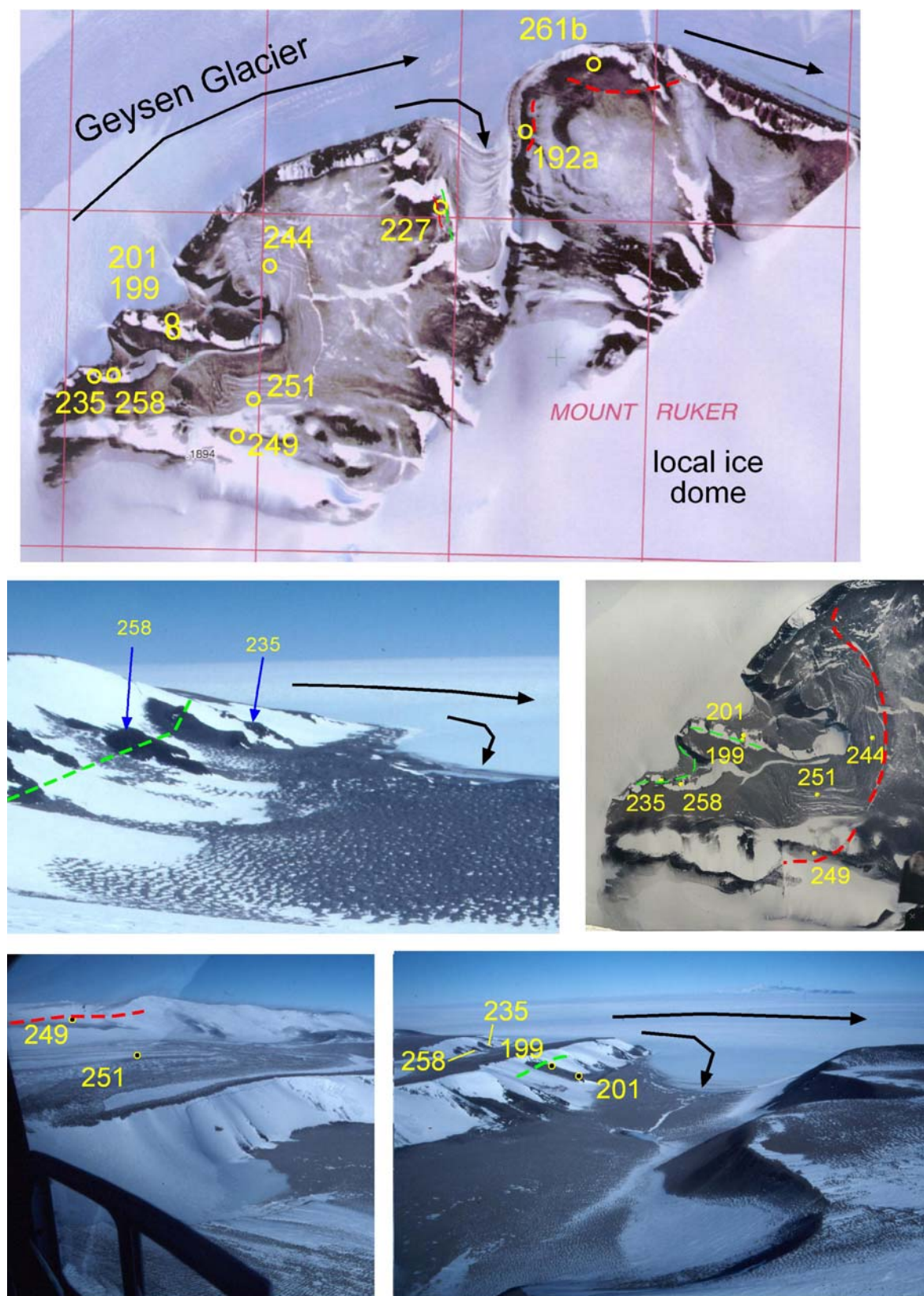
Fig DR3a: Vertical and oblique aerial view of sample sites at Mt Ruker. Red dashed line indicates maximum height/distance from outlet glacier of slightly weathered debris. Green line indicates more subtle demarcation line, beyond which unweathered debris are no longer observed.

Fig DR3b: Samples from plateau surface, resting on hummocky ice cored diamict (Ruk-244,1502 m; Ruk-249, 1655 m, Ruk-251, 1525m) , or a diamict/felsenmeer mixture (Ruk-227, 1280 m; Ruk-261 b, 1239 m).

Fig DR3c: Samples collected from scattered debris on bedrock spurs. Samples Ruk-192a, Ruk-199a, Ruk-235a and 258a shown. Photographs of Ruk-201 and 235b were ruined by overexposed film but have very similar field positions to those displayed here. Note the distinct limit of glacial debris (indicated by red arrow) at site Ruk-192a – this corresponds to the limit of 'lightly weathered' debris, rather than the lower, 'unweathered' debris that is inferred to be the local LGM at Mt Ruker.
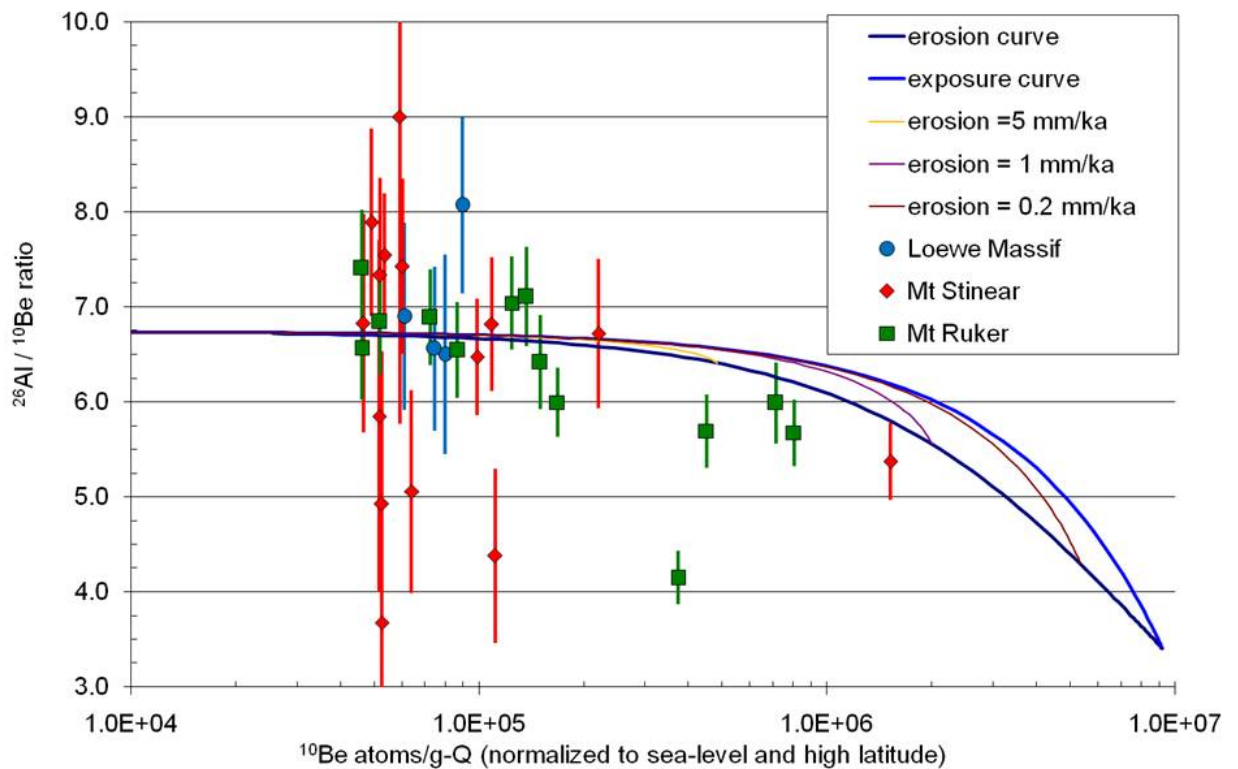
Data Repository Figure DR4

Dual isotope plot of $^{10}Be/^{26}Al$ ratio versus ^{10}Be concentration (normalised to sea-level and high latitude). Note the contrast between young samples (n=26) with ages <35 ka (those with ^{10}Be concentrations <2 x 10^5 atoms/g-Q) and older samples (n=7) (those with ^{10}Be concentrations > 2 x 10^5 atoms/g-Q). All but 4 of 26 samples in the younger population plot within the constant exposure region (not including 2 Mt Stinear samples with large error bars due to low statistic ^{26}Al AMS measurement). In contrast, of the 7 in the older population (one with ^{10}Be age only), 3 plot below the constant erosion curve, suggesting that although situated at or below the demarcation weathering limit which locates the local LGM elevation, a far larger fraction of the older population have been subjected to at least one cycle of exposure, burial and re-exposure. We therefore conclude that the older population provide no real indication for the timing of ice retreat.
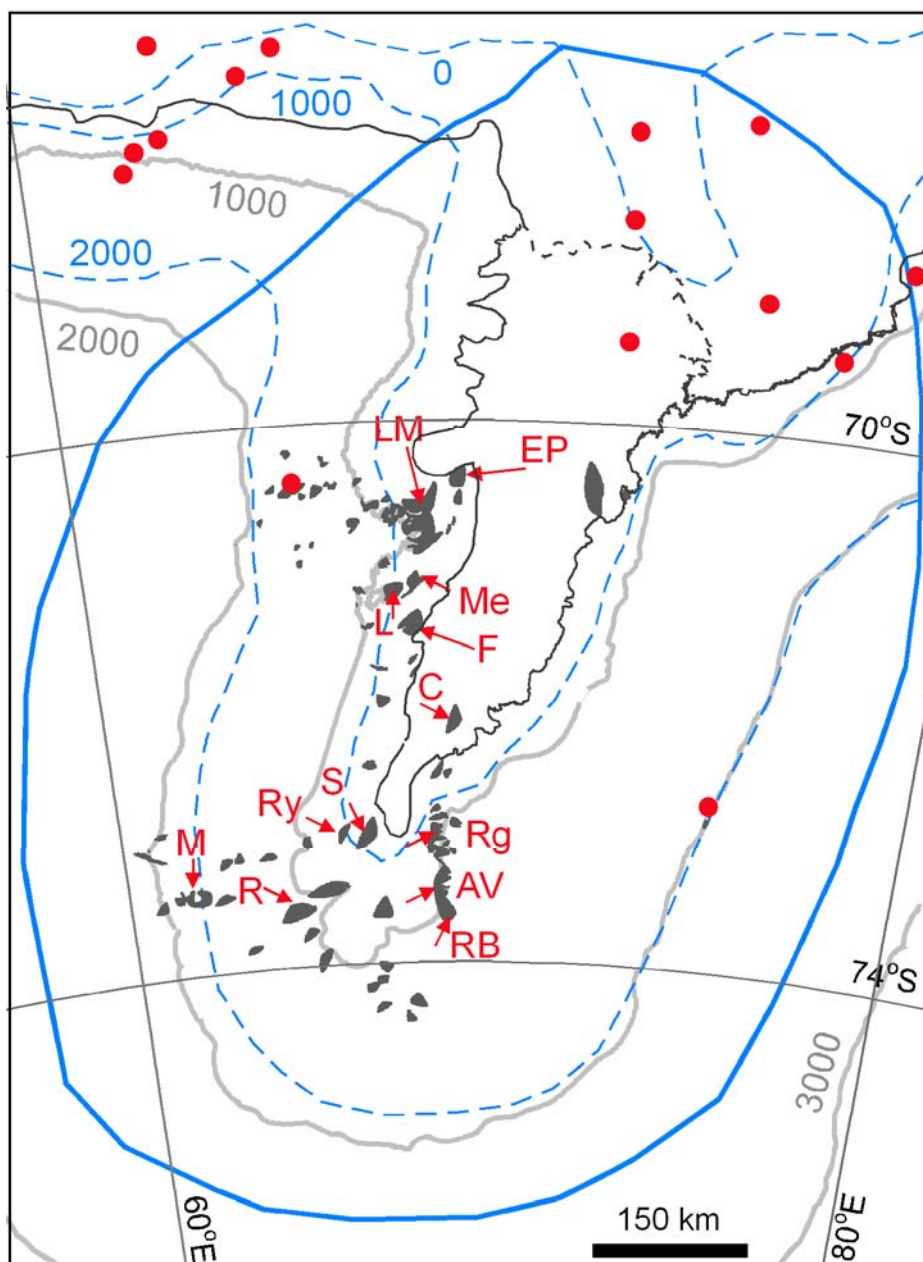
Data Repository Figure DR5

Reconstruction of the maximum height of the lower LG-AIS since the onset of the global Last Glacial Maximum. Red arrows indicate the ten locations used to construct the profile in Figure 4 (of main text), grouped as follows: Mt Menzies (M), Mt Ruker (R), Rimmington Bluff (RB), Accidental Valley (AV), Mt Rymill (Ry) and Mt Stinear (S), Rofe Glacier (Rg), Clemence Massif (C), Fisher Massif (F), Mt Lanyon (L) and Mt Meredith (Me), Loewe Massif (LM) and Else Platform (EP). Red dots indicate other locations where the maximum height or extent of the ice sheet during and since the global Last Glacial Maximum has been constrained and published previously using the following references: Mabin, 1992 (Manning and Fisher Massif); Domack et al., 1998, Harris and O'Brien, 1998,

Taylor and McMinn, 2002 (Prydz Bay region); Zwartz et al., 1998 (Vestfold Hills); Hodgson et al., 2001 (Larsemann Hills); Hemer and Harris, 2003 (Amery Ice Shelf); Leventer et al., 2006 (Mac.Robertson Land Shelf); Mackintosh et al., 2007 (Framnes Mts); Lilly et al., 2010 (Groves Mts); Black line indicates modern coastline or grounding line, dashed black line indicates the calving margin of the Amery Ice Shelf. Grey lines indicate modern ice contours (in metres). Dashed blue lines indicate inferred maximum paleo-ice contours (in metres), estimated from data presented in this paper and the preceding references. The solid blue line indicates area used to calculate maximum difference in grounded ice volume since the LGM and today. In the northern part of the region, the blue line follows (a) the LGM grounding line, (b) the ice divide between the LG-AIS and the remainder of the ice sheet commencing at the grounding line to where the ice divide reaches 2500 m elevation, and (c) the LGM 2500 m ice contour within the LG-AIS.

DR Figure DR6
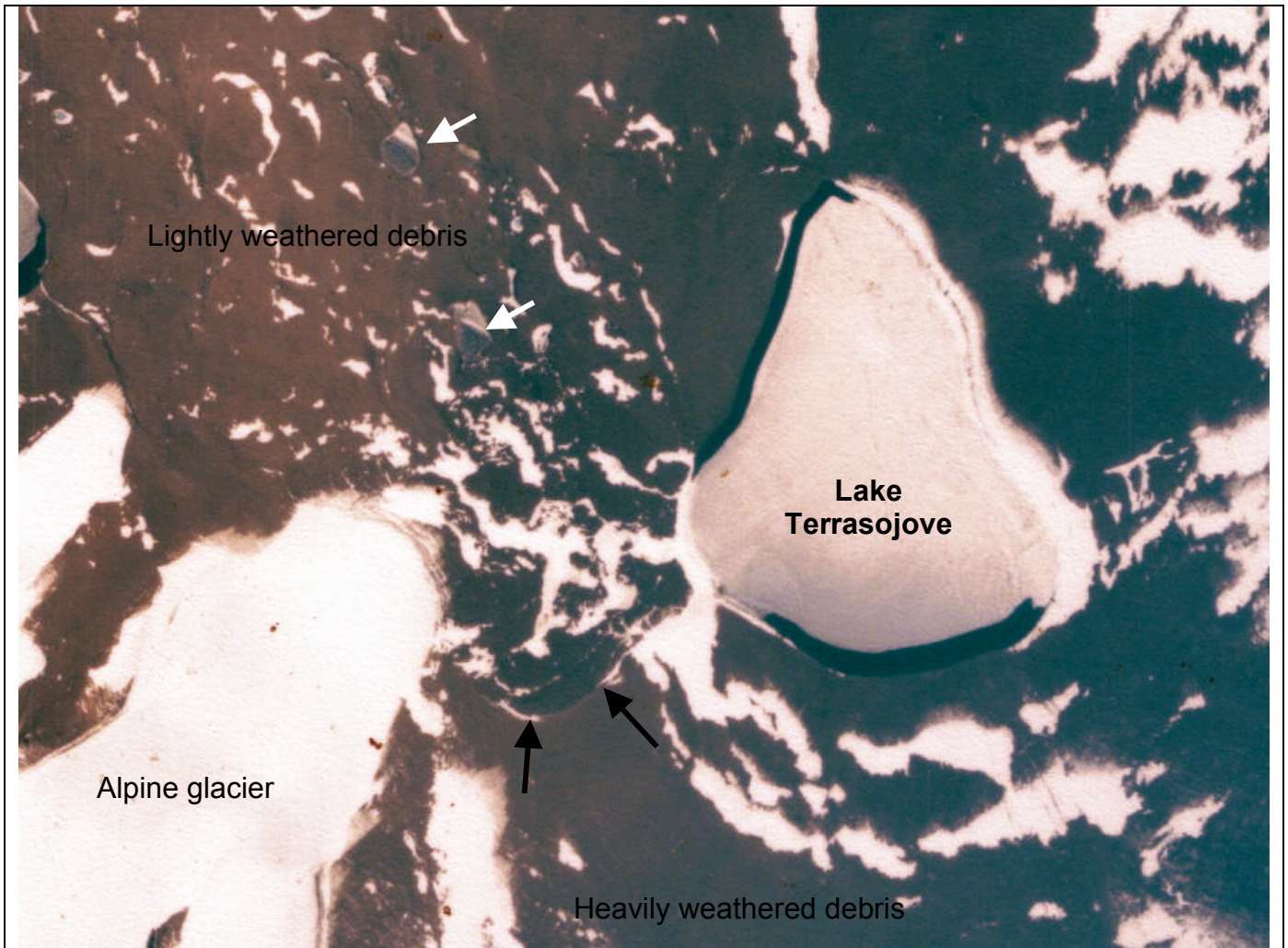
(a) Vertical aerial photograph (CAS/C 8575, Run 26, Photo 136, 8/10/74) of the limit of lightly weathered debris (black arrows) near Lake Terrasovoje at Loewe Massif. Note the hummocky nature of the lightly weathered debris (highlighted by the remnant snow patches), and the small lakes (white arrows) trapped in surface irregularities of the sheet. The heavily weathered debris has a surface morphology similar to the area of patterned ground in DR Figure 6b. Image is ~ 3 km across.
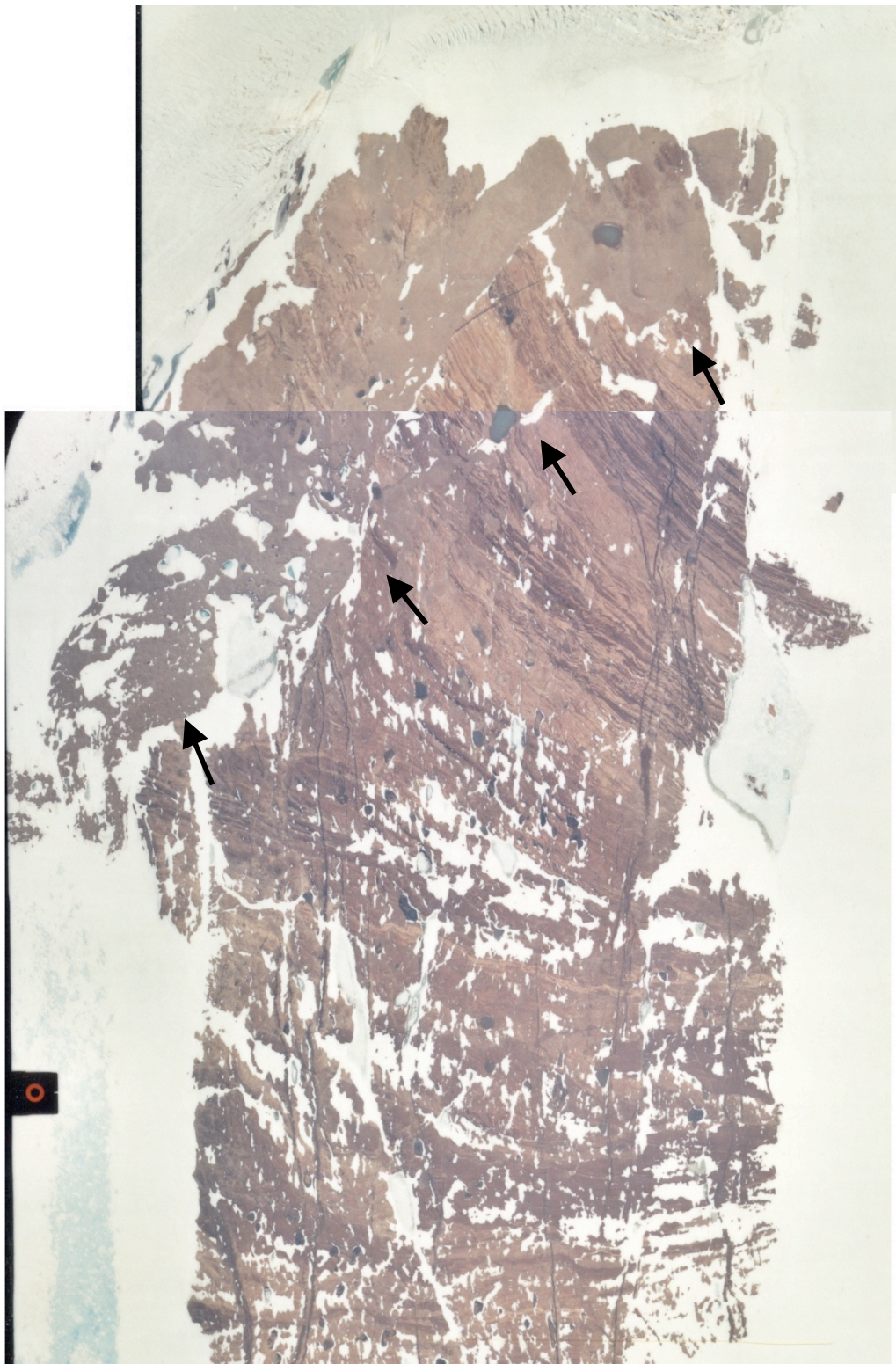
(b) Oblique aerial photograph mosaic (ANTC 1059, Run 1, Frames 21 and 23, 25/1/98) of the north-eastern tip of Else Platform. Arrows mark the southernmost extent of glacially deposited sediment. All (surface) expressions of this sediment are lightly weathered. The fine scale banding (NW-SE in the north, E-W in the south) denotes the structural grain of the banded gneiss bedrock at this site. The image is 3 km across.
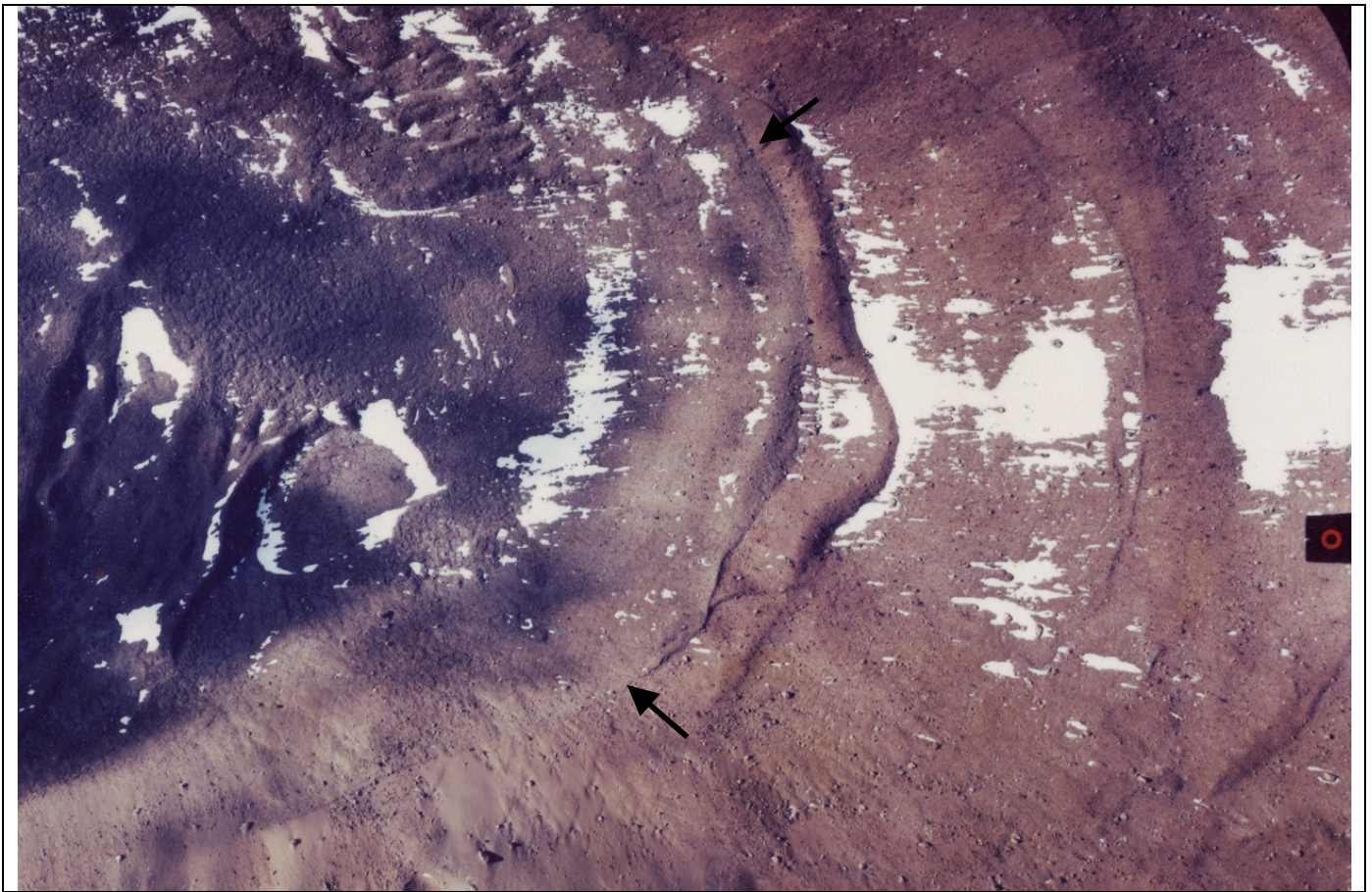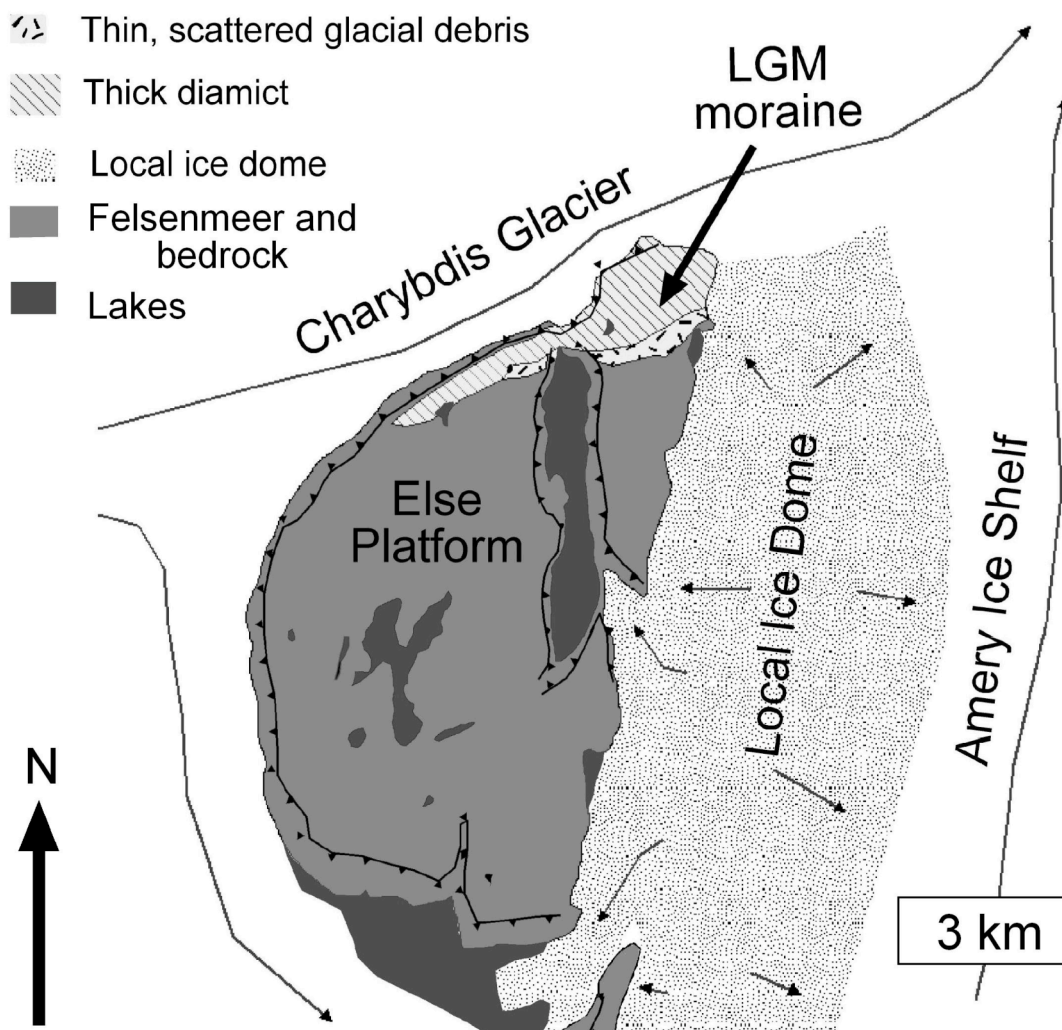
(c) Vertical aerial photograph (ANTC1058, run 3, frame 92, 24/1/98) of the limit of lightly weathered debris (black arrows) at Accidental Valley. Boulders on the moraine ridges to the right (west) of this sheet all provided ^{10}Be ages of > 400 ka (White, 2007). Image is ~ 800 m wide.

DR Figure DR7

Surficial stratigraphy of Else Platform at the junction of the Charybdis Glacier and the main ice stream of Lambert Glacier, 10 km east of the Loewe Massif. The main Charybdis Glacier LGM moraine (light grey with diagonal stripes) covers the northern margin of the platform, with a thin scatter of cobbles and diamict with a similar degree of weathering extending a few hundred metres further from the glacier (light grey with black stipples). Ice flow directions are indicated by thin black arrows. The remaining ice-free region (medium grey) consists of heavily weathered bedrock and locally derived felsenmeer, and glacially transported debris is absent. The Charybdis LGM moraine displays no evidence of glacial overriding or cross-cutting moraines from ice derived from the northerly flow direction of the modern Amery Ice Shelf, indicating that ice from the trunk stream of the Lambert Glacier-Amery Ice Shelf System was not present at this site during or following the LGM.